

Citation for published version:

Pérez-Mendoza, M, González, J, Ferreiro-Rangel, CA, Lozinska, MM, Fairén-Jiménez, D, Düren, T, Wright, PA & Seaton, NA 2014, 'Pore-network connectivity and molecular sieving of normal and isoalkanes in the mesoporous silica SBA-2', *The Journal of Physical Chemistry C*, vol. 118, no. 19, pp. 10183-10190.
<https://doi.org/10.1021/jp502390p>

DOI:

[10.1021/jp502390p](https://doi.org/10.1021/jp502390p)

Publication date:

2014

Document Version

Peer reviewed version

[Link to publication](#)

This document is the Accepted Manuscript version of a published work that appeared in final form in The Journal of Physical Chemistry C, copyright (C) American Chemical Society after peer review and technical editing by the publisher. To access the final edited and published work see <http://doi.org/10.1021/jp502390p>

University of Bath

Alternative formats

If you require this document in an alternative format, please contact:
openaccess@bath.ac.uk

General rights

Copyright and moral rights for the publications made accessible in the public portal are retained by the authors and/or other copyright owners and it is a condition of accessing publications that users recognise and abide by the legal requirements associated with these rights.

Take down policy

If you believe that this document breaches copyright please contact us providing details, and we will remove access to the work immediately and investigate your claim.

This document is confidential and is proprietary to the American Chemical Society and its authors. Do not copy or disclose without written permission. If you have received this item in error, notify the sender and delete all copies.

Pore-Network Connectivity and Molecular Sieving of Normal and Iso-Alkanes in the Mesoporous Silica SBA-2

Journal:	<i>The Journal of Physical Chemistry</i>
Manuscript ID:	jp-2014-02390p
Manuscript Type:	Article
Date Submitted by the Author:	09-Mar-2014
Complete List of Authors:	Perez-Mendoza, Manuel; University of Granada, Departamento de Quimica Inorganica González, Jorge; Escuela de ciencias químicas, Universidad de Colima Ferreiro-Rangel, Carlos; University of Edinburgh, School of Engineering Lozinska, Magdalena; University of St Andrews, Chemistry Fairen-Jimenez, David; University of Cambridge, Dept. of Chemical Engineering & Biotechnology Düren, Tina; University of Edinburgh, School of Engineering Wright, Paul; University of St. Andrews, Chemistry Seaton, Nigel; University of Edinburgh,

SCHOLARONE™
Manuscripts

1
2
3
4
5
6
7
8
9
10
11
12
13
14
15
16
17
18
19
20
21
22
23
24
25
26
27
28
29
30
31
32
33
34
35
36
37
38
39
40
41
42
43
44
45
46
47
48
49
50
51
52
53
54
55
56
57
58
59
60

Pore-Network Connectivity and Molecular Sieving of Normal and Iso-Alkanes in the Mesoporous Silica SBA-2

Manuel Pérez-Mendoza^{,†}, Jorge González^{‡,§}, Carlos A. Ferreiro-Rangel[§], Magdalena M.*

Lozinska[‡], David Fairén-Jiménez^{§,¶}, Tina Düren[§], Paul A. Wright[‡], Nigel A. Seaton^{§,}*

[†] Departamento de Química Inorgánica, Facultad de Ciencias, Universidad de Granada, 18071
Granada, Spain.

[§] Institute for Materials and Processes, School of Engineering, The University of Edinburgh,
King's Buildings, Edinburgh, EH9 3JL, UK, UK.

[‡] EaStCHEM School of Chemistry, University of St Andrews, North Haugh, St Andrews, Fife,
KY16 9ST.

[§] Facultad de Ciencias Químicas, Universidad de Colima, Colima, 28040, México

KEYWORDS: SBA-2 structure, normal and iso-alkane separation, pore-network connectivity,
molecular sieving, percolation, molecular simulation, adsorbent design.

1
2
3 ABSTRACT: We have studied the adsorption of n-butane and iso-butane in the mesoporous
4 silica SBA-2. Our work has two purposes: (i) to better understand the structure of the material,
5 and in particular the impact of calcination on the evolution of the pore network; and (ii) to
6 investigate our ability to tune the structure of SBA-2 to separate normal and iso-alkanes by
7 molecular sieving. By a combination of experimental adsorption measurements, molecular
8 simulation, and percolation analysis, we determined the evolution of the sizes of the pores and
9 the connectivity of the pore network as the calcination temperature increases. For a certain range
10 of calcination temperatures, the pore network drops below its percolation threshold for iso-
11 butane, while allowing the percolation of n-butane, giving an extremely high selectivity for n-
12 butane over iso-butane. This suggests that tuning the window size of SBA-2 and other structured
13 mesoporous materials of this general type has the potential to generate optimized adsorbents for
14 particular applications.
15
16
17
18
19
20
21
22
23
24
25
26
27
28
29
30
31

32 33 1. INTRODUCTION

34
35 Since their discovery in the early nineties¹⁻², periodic mesoporous silicas (PMSs) have become
36 one of the most versatile families of materials with applications in, for example, gas separation,
37 adsorption, controlled drug release, shape-selective catalytic processes and sensing³⁻⁵. The way
38 they are synthesized, using a precursor solution with a silica source and a liquid-crystal phase
39 formed by a surfactant which serves as a template for the porous material, followed by the
40 calcination of the resultant silica network, is the origin of their versatility^{1-2,6}. Firstly, the
41 template generates a well-defined long-range order in the structure, whilst at an atomic level the
42 material is non-crystalline. The use of different precursor solutions and reaction conditions leads
43 to different structures and PMSs exist with mono-, bi-, or tri-dimensional pore networks and with
44 a wide range of pore sizes⁷⁻⁹. The pore size and connectivity of the network affects the
45
46
47
48
49
50
51
52
53
54
55
56
57
58
59
60

1
2
3 equilibrium and dynamics of molecular processes occurring within the pore space such as the
4
5 adsorption and diffusion of gases. Secondly, the surface chemistry of the pores can be modified
6
7
8 by lining with organic groups and metals either by in situ co-condensation or by post-synthesis
9
10 grafting¹⁰⁻¹¹, changing for example the hydrophilicity and acidity of the materials, with all the
11
12 implications this has for their possible uses in selective adsorption and catalysis.
13
14

15 SBA-2 is a PMS with a three-dimensional pore network¹²⁻¹³. One of the distinctive features of
16
17 SBA-2 is that the topology of the network is formed by spherical cavities arranged in either
18
19 hexagonal close-packed (hcp) or cubic close-packed (ccp) networks, with diameters in the
20
21 mesopore size-range that are interconnected by smaller, cylindrical channels, with sizes in the
22
23 micropore size-range¹²⁻¹⁴. (The ccp material is strictly designated STAC-1, but in this paper we
24
25 use for convenience the term SBA-2 to refer to both materials. In practice, samples typically
26
27 contain materials with both structures, intergrown, although recently both pure ccp and pure
28
29 hexagonal close packed structures have been prepared using a costructure directing agent and
30
31 gemini surfactant under closely controlled conditions¹⁵⁻¹⁶). Thus, the pore structure combines the
32
33 large volume associated with the cage-like pores with the selectivity with respect to molecular
34
35 size and shape of the narrow microporous channels. This combination is attractive for
36
37 applications such as adsorptive separations and shape-selective catalysis.
38
39
40
41
42

43 The channels appear to originate in the close proximity of the spherical micelles during the
44
45 synthesis process, leading to a concentration of water molecules at the interface, and a
46
47 corresponding tendency for the silica condensation in this region to be relatively slight¹⁷. We
48
49 have also suggested that the channels might be further developed when the synthesized material
50
51 is calcined to remove the surfactant¹⁸. It is thus unlikely that the cages will be connected
52
53 following a completely regular pattern and that all the channels will have the same size. It is
54
55
56
57
58
59
60

1
2
3 more likely that the calcination process will have an important effect on how these channels are
4 formed and, hence, on the connectivity of the porous network – that is, on the number and size of
5 the channels connecting the cavities. As the connectivity has a direct effect on the accessibility of
6 the channels connecting the cavities. As the connectivity has a direct effect on the accessibility of
7 adsorptives to the pores, this will condition the performance of SBA-2 material as an adsorbent
8 or catalyst support. Therefore, establishing and controlling the relationship between preparation
9 and performance is crucial from the materials design point of view.
10
11

12
13
14
15
16
17 In a previous communication¹⁴, we showed that a model based on a pore size distribution
18 (PSD) of cylinders (representing the interconnecting channels) and spheres (representing the
19 spherical cavities) is able to describe and accurately predict the adsorption of methane and ethane
20 on SBA-2 using the grand canonical Monte Carlo (GCMC) simulation method. In a subsequent
21 paper¹⁸, we showed that percolation theory, together with the PSD analysis, can be used to
22 understand the accessibility of the pore network to molecules of different sizes and shapes, and
23 hence to evaluate the connectivity of the network. The results indicated a much lower effective
24 coordination number for the cavities than expected from the geometric structure of the system.
25
26 The network was sufficiently well connected that it was above the percolation threshold for both
27 species studied, nitrogen and ethane. That is, both species could gain access to all macroscopic
28 regions of the material, though not necessary to every individual cavity. The effective
29 coordination numbers experienced by the two species were very different, however: 4.9 for
30 nitrogen and 1.8 for ethane. (The value for ethane is just above the percolation threshold for the
31 SBA-2 network, which percolates when the effective coordination number is 1.44¹⁹).
32
33
34
35
36
37
38
39
40
41
42
43
44
45
46
47
48
49

50
51 The purpose of the present work is to improve our understanding of the pore structure of SBA-
52 2 by applying the adsorption-percolation analysis to larger adsorptives with different shapes, n-
53 butane (C4) and iso-butane (isoC4), and to use this analysis to understand the relationship
54
55
56
57
58
59
60

1
2
3 between the temperature of calcination and the pore structure. This is important for two reasons.
4
5 Firstly, by using larger molecules than in our earlier study¹⁸ we gain further insights into the
6
7 effect of the manufacturing process on the pore structure of SBA-2. Secondly, we are interested
8
9 in the potential of SBA-2 for shape-selective adsorption in applications in which a high
10
11 adsorption capacity is important. The C₄/isoC₄ system is an example of an important class of
12
13 industrial processes in which normal and iso-alkanes are separated.
14
15
16
17
18
19

20 2. EXPERIMENTAL SECTION

21
22 The SBA-2 samples were prepared at room temperature and alkaline pH using a gemini
23
24 quaternary ammonium surfactant as template. A complete description of the preparation
25
26 methodology has been previously reported¹². Different batches calcined at 700, 800 and 900 °C
27
28 were prepared to study the influence of calcination temperature in the structure. A solvent-
29
30 extracted sample (with no calcination) was also prepared. Further samples calcined at 550 and
31
32 820 °C were prepared for the study of mixture adsorption.
33
34
35

36
37 Powder X-ray diffraction patterns were collected in transmission mode in the form of powder
38
39 supported in 0.7 mm quartz glass capillaries. Measurements were made at ambient temperature
40
41 using monochromated Cu K_{α1} radiation, $\lambda = 1.54056 \text{ \AA}$, on a STOE Stadi/p diffractometer.
42
43

44
45 Transmission electron microscopy (TEM) micrographs were taken using a JEOL-JEM 2011
46
47 electron microscope equipped with a CCD Gatan digital camera operating at 200 keV. Samples
48
49 were ground before being dispersed in acetone then deposited onto a holey carbon film,
50
51 supported on a Cu grid.
52

53
54 The adsorption of nitrogen at 77 K and C₄ and isoC₄ at 268 K was measured from 0-1 bar
55
56 using a Hiden IGA automated gravimetric analyzer. Typically 10-25 mg of sample were used in
57
58
59
60

1
2
3 the determination of each isotherm. Samples were degassed at 383 K for 3h under vacuum and
4
5 cooled to room temperature before the dry mass was set. For nitrogen the sample chamber was
6
7 immersed in liquid nitrogen, whereas for the butanes the temperature of the sample chamber was
8
9 regulated by a Grants Optima GR150 thermostatic recirculating water bath.
10
11

12 Mixture adsorption experiments were carried out on a bench-scale open-flow
13
14 adsorption/desorption system. The system has been described previously²⁰. In essence, a mixture
15
16 of a constant composition is allowed to flow past the sample until the outlet composition of the
17
18 gas reaches steady-state, at which point adsorption equilibrium is judged to have been attained.
19
20 The adsorbed phase is then desorbed by heating to 423 K, and collected in a container cooled to
21
22 77 K. The amount and composition of the adsorbate is then measured. In these experiments, a
23
24 1:1 C4/isoC4 gas mixture was allowed to flow past the sample at 268 K and 0.8 bar.
25
26
27
28
29
30
31

32 3. ADSORPTION-PERCOLATION ANALYSIS

33

34 The essence of our approach is to treat separately two aspects of adsorption on this material,
35
36 each of which relates to a different length scale: the local adsorption equilibrium within
37
38 individual pores; and the effect that the pore network has on the accessibility of those pores to
39
40 different adsorptive species. As in our previous work^{14,18}, the channels and cavities in SBA-2 are
41
42 represented by, respectively, cylindrical and spherical pores, with the pores having a regular,
43
44 atomistic surface. The adsorption of a particular species in a particular pore (either a cavity or a
45
46 channel, with a specified diameter) is modeled using grand canonical Monte Carlo (GCMC)
47
48 simulation, which generates a local adsorption isotherm, i.e. the equilibrium amount adsorbed as
49
50 a function of pressure. At this level of the model, the pores are considered to be independent of
51
52
53
54
55
56
57
58
59
60

1
2
3 each other; that is, the fact that in reality the pores are connected together in a network is
4
5 ignored. A complete description of the GCMC method used can be found in our earlier paper¹⁴.
6
7

8 It should be noted that a more rigorous treatment of adsorption on SBA-2 would treat the pore
9
10 network in an integral way, that is, without separately defining cavities and channels as “building
11
12 blocks” of the network. We have recently published an account of this approach, using a kinetic
13
14 Monte Carlo (kMC) method to simulate the synthesis of SBA-2 (and the closely related material
15
16 STAC-1)¹⁷. Using this approach, the connections between the cavities arise naturally from the
17
18 simulation. Both the individual cavities and the connections between them are, naturally, rather
19
20 irregular, whilst in a statistical sense the cavities remain spherical and their connections have an
21
22 approximately circular cross-section (though their cross-sectional area varies along their axis).
23
24

25
26 The model materials generated by kMC simulation - which we take to be a good representation
27
28 of the real materials - thus support the use of spherical cavities in the present, simpler model.
29
30

31 The representation of the connections generated by kMC simulation as cylinders in the present
32
33 model is less exact, but the present approach captures the essence of the connections as short,
34
35 narrow elements with small but finite adsorption capacity. Whilst kMC simulation gives
36
37 powerful insights into the synthesis and properties of the real materials, the computational
38
39 demands of that approach are far too great for that method to be used for the extensive
40
41 adsorption-percolation analysis reported here.
42
43
44

45 In our simulations, nitrogen was modeled as a two-site Lennard-Jones (LJ) molecule with a
46
47 quadrupole, following Kjems and Dolling²¹. C4 and isoC4 were modeled as four-site molecules,
48
49 with the CH₃, CH₂ or CH groups represented by individual LJ sites. The potential parameters are
50
51 given in Table 1. The silicon atoms are neglected, with their small contribution to the adsorption
52
53 potential²² implicitly included in the potential parameters of the oxygen atoms.
54
55
56
57
58
59
60

The impact of the pore network on the adsorption - and in particular the effect of constrictions in the network on the accessibility of the pores to different adsorptive species - is modeled using percolation theory. To transform the problem of adsorption on SBA-2 into percolation terms we note that the accessibility of the network is controlled by the channels (“bonds”, in the language of percolation), as the cavities (“sites”, in percolation terms) are much larger than both the adsorptive species studied. The channels are of a comparable size to the adsorptive species, so that some permit the passage of both butane isomers (C4 and isoC4), some permit only the passage of the less bulky species (C4) and some permit the passage of neither species. Indeed, our earlier work¹⁸ showed that some channels in SBA-2 are too small even to permit the passage of nitrogen, and that some of the channels that would correspond to a fully coordinated network might even be completely absent.

Table 1: Potential parameters for the fluids and SBA-2.

molecule	ϵ/k_B , K	σ , Å	quad. Moment, C·m ²	bond length, Å
N ₂ (2 CLJ) ²¹	33.4	3.383	-3.712	0.923
C ₄ (CH ₃) ²³	88.1	3.905	-	1.53
C ₄ (CH ₂) ²³	59.4	3.905	-	1.53
isoC ₄ (CH ₃) ²³	80.5	3.910	-	1.53
isoC ₄ (CH) ²³	40.3	3.850	-	1.53
O	185.0	2.708	-	

Adsorption on SBA-2 is an example of percolation on a regular lattice. In the simplest form of lattice percolation, the individual elements are either the sites or the bonds. In “site percolation”, the network percolates if sufficient sites are occupied so that a connected network of sites spans the network. One then quantifies, for example, the proportion of the sites that are in the

1
2
3 percolating cluster of sites – the “accessibility” of the sites. In “bond percolation”, the network
4
5
6 percolates if sufficient bonds are occupied, and one calculates the accessibility of the bonds.
7
8 Adsorption in SBA-2 corresponds to a more complex percolation problem in which both sites
9
10 and bonds must be considered. The bonds determine the accessibility of the network, while both
11
12 the sites and the bonds contribute to adsorption. In percolation terms, a site or bond is defined to
13
14 be “occupied” if it is large enough to accommodate the species of interest, so that a percolating
15
16 cluster of sites and bonds would allow adsorption of that species. In the study of the adsorption
17
18 of nitrogen, C4 and isoC4 on SBA-2, all the sites are occupied as they are larger than all these
19
20 species; the site occupation probability, $p^s = 1$. In contrast, only some of the bonds are occupied,
21
22 i.e. are large enough to allow the passage of the species; the bond occupation probability, $p^b < 1$.
23
24 Thus, adsorption in the channels corresponds to bond percolation, while adsorption in the
25
26 cavities corresponds to what is sometimes termed “site percolation in the bond problem”¹⁹. In the
27
28 latter case, the network elements of fundamental interest are the sites, while their accessibility is
29
30 controlled by the bonds; in adsorption terms, adsorption in the cavities is controlled by passage
31
32 of the adsorptive species through the channels.
33
34
35
36
37
38

39 The network variable that controls the accessibility of both the sites and the bonds (and hence
40
41 the overall adsorption) is thus the bond occupation probability, p^b . This has a different value,
42
43 $p^{b,i}$, for each species, i . $p^{b,i}$ is related to the mean number of channels per cavity that are large
44
45 enough to accommodate that species (the “effective” coordination number), z^i , by

$$z^i = Zp^{b,i} \quad (1)$$

46
47
48 where Z is the coordination number of the network; $Z = 12$ for both hcp and ccp networks. The
49
50 percolation behavior of a network with $Z = 12$ has been computed by Yanuka¹⁹ for both bond
51
52 percolation and “site percolation in the bond problem”. [Yanuka studied only the ccp network.
53
54
55
56
57
58
59
60

1
2
3 However, as the percolation properties of a network depend mainly on the dimensionality and
4 coordination number, and only to a small extent on other aspects of the topology²⁴, Yanuka's
5 results are applicable to both the ccp and hcp forms of the SBA-2 network].
6
7

8
9
10 The first step in the connectivity analysis¹⁸ is to determine the accessibility of the sites to each
11 species. This is done by using the simulated adsorption isotherms to obtain the pore size
12 distribution (PSD) of the cavities. By using nitrogen, C4 and isoC4 in turn, we obtain three
13 different PSDs, each describing the portion of the pore network that is probed by that species.
14 IsoC4 is more bulky than C4, which in turn is more bulky than nitrogen, so the PSDs are
15 expected to show peaks that diminish in magnitude in the order isoC4 > C4 > nitrogen.
16
17
18
19

20 We root the present analysis in information about the accessibility of the SBA-2 pore network
21 from our earlier work¹⁸. In that work, the SBA-2 sample was prepared by post-synthesis
22 calcination at 550 °C. The nitrogen adsorption isotherm of that material is almost identical to
23 that of the solvent-extracted sample in the present work (reflecting the relatively mild effect of
24 calcination at that relatively low temperature, Figure S1). We are thus able to use the bond
25 occupation probability for nitrogen, $p^{b,n} = 0.41$ (corresponding to $z^n = 4.9$) from that study and
26 apply it to the present solvent-extracted sample. Our adsorption-percolation analysis thus
27 measures changes in the connectivity of the pore network of the various calcined samples, as
28 experienced by different species, relative to the datum of nitrogen adsorption in the solvent-
29 extracted sample. The fraction of cavities accessible to species i , $P^{s,i}$ is related to the PSD by:
30
31
32
33
34
35
36
37
38
39
40
41
42
43
44
45
46
47

$$48 \quad P^{s,i} = \frac{\int_0^\infty f^i(r) dr}{\int_0^\infty f^n(r) dr} \quad (2)$$

49 where $f^i(r) = dN^i/dr$: N^i is the number of pores, so that $f^i(r)$ is the probability density function for
50 the number of pores as a function of pore radius. $f^n(r)$ is the “reference” distribution, measured
51 using the adsorption of nitrogen on the solvent-extracted sample.
52
53
54
55
56
57
58
59
60

1
2
3 The precise definition of the PSD used in eq (2) requires some discussion. The conventional
4 definition of the PSD, and the form that is obtained directly from adsorption measurements, is
5 the distribution of the pore volume, rather than the pore number, as a function of pore radius; for
6 the spherical cavities considered here, $dN^i/dr = 1/r^3 \cdot dV^i/dr$. For a given material, the set of
7 cavities explored by different adsorptive species differ in their connections to other pores, but not
8 – in a statistical sense – in their size. The ratio of the numbers of pores accessible to different
9 species is therefore the same as the ratio of the pore volumes accessible to different species. In
10 such a case, eq (2) could identically be written in terms of dV^i/dr rather than dN^i/dr . Indeed, this
11 approach was taken in our earlier paper¹⁸. However, when comparisons are being made between
12 different materials – in our case, samples of SBA-2 calcined at different temperatures, or solvent-
13 extracted – the relationship between accessible volume and accessible number of pores is
14 different for different materials. The materials represented by the numerator and the denominator
15 of eq (2) are different, so the fundamentally correct pore number distribution, dN^i/dr , must be
16 used.

17
18
19
20
21
22
23
24
25
26
27
28
29
30
31
32
33
34
35
36
37
38
39
40
41
42
43
44
45
46
47
48
49
50
51
52
53
54
55
56
57
58
59
60
The PSD analysis was carried out by solving the adsorption integral equation using the
numerical approach of Davies and Seaton²⁵. This relates the overall adsorption, as measured in
an experiment, to adsorption in individual pores, represented by molecular simulations of
adsorption on model cylindrical and spherical model pores of different sizes.

Once $P^{s,i}$ has been obtained, we use Yanuka's results for site percolation in the bond problem¹⁹
(shown in Figure 1) in the cavities to obtain $p^{b,i}$, which in turn gives the effective coordination
number for this species, z^i .

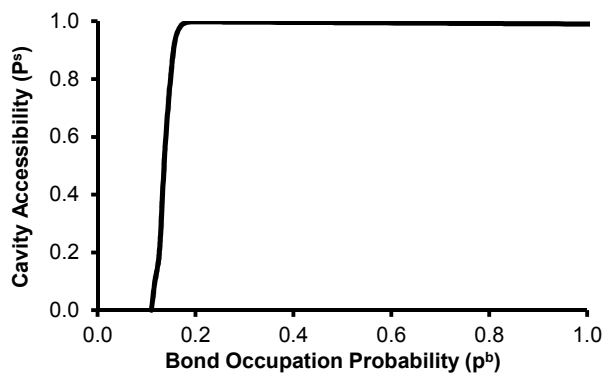


Figure 1: Yanuka's function for site percolation in the bond problem in fcc lattice¹⁹.

Thus, the problem of characterizing the connectivity of our SBA-2 network is reduced to the determination of the fraction of cavities accessible to the different adsorptive species under study, which in turn requires the determination of the PSD of the portion of the pore network that is probed by those species. In our work, the PSDs of the portions of the network accessible to nitrogen, butane and isobutane were obtained by analyzing the experimental adsorption isotherms of those species (at 77 K, for nitrogen, and 268 K for C4 and isoC4).

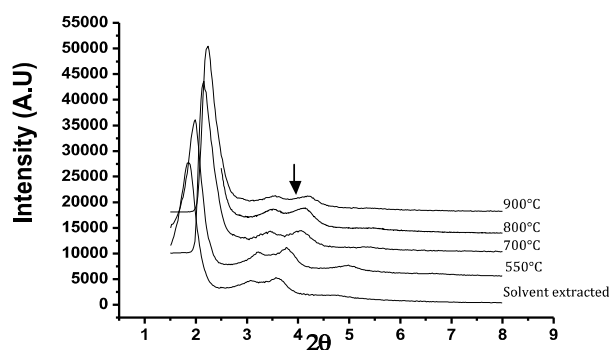
In summary, the steps in the adsorption-percolation analysis of each sample are as follows:

1. For each adsorptive, the PSD is obtained using nitrogen, C4 and isoC4.
2. The PSDs are integrated using Eq. (2) to obtain $P^{s,i}$.
3. The data of Figure 1 are used to obtain $p^{b,i}$.
4. The effective coordination number experienced by each species is obtained from Eq. (1).

4. RESULTS AND DISCUSSION

XRD analysis of the samples calcined at different temperatures shows that the symmetry of the network is preserved through the calcination process even for the highest calcination temperature (Figure 2). High resolution transmission electron microscopy confirmed that the ordered close packed array of cages remained after each calcination²⁶. Huo et al.²⁷ reported that silicate SBA-2

1
2
3 material was thermally stable up to 800 °C. It is clear from our XRD and TEM analysis that the
4
5 SBA-2 is actually stable up to 900 °C. Nevertheless, the diffraction maxima shift progressively to
6
7 higher angles with the increase in calcination temperature, indicating a systematic contraction of
8
9 the unit cell. TEM micrographs of the solids show large cubic domains corresponding to cubic
10
11 close packed spherical pores (Figure S2). The absence of any well-defined $(103)_{\text{hex}}$ reflection in
12
13 the XRD patterns, which is expected for the hexagonal close packed array but not for the cubic
14
15 stacking, also agree with a major proportion of cubic stacking. Indexing the patterns according to
16
17 the cubic ($Fm\bar{3}m$) structure, the unit cell parameter, a , changes from 81.5 for the extracted
18
19 sample, to 70 Å for the sample calcined at 900 °C.
20
21
22
23
24



40
41
42
43
44
45
46
47

Figure 2: XRD analysis of SBA-2 samples calcined at different temperatures. The solid black arrow indicates the theoretical position of the $(103)_{\text{hex}}$ Bragg reflection on the solid calcined at 900°C.

48
49
50
51
52
53
54
55
56
57
58
59
60

The decrease of the a unit-cell parameter is almost linear with the calcination temperature and represents a 35% volume contraction for the sample calcined at the highest temperature. A summary of these data can be found in Table 2. Evidence on the progressive condensation of the amorphous walls of SBA-2 with increasing temperature has also been found by Ferreiro-Rangel *et al.* using ^{29}Si MAS-NMR¹⁷.

Table 2: XRD cell parameters for the SBA-2 samples calcined at different temperatures.

Temperature of calcination, °C	a [Å]
solvent-extracted	81.5
700	72.8
800	71.6
900	70.0

The contraction of the unit cell is also clearly evidenced by the experimental isotherms for the adsorption of nitrogen at 77 K (Figure 3). All these isotherms have two clear steps. The first occurs at low pressure and is related to adsorption in the regions of the pore space where the adsorption energy is high – that is, in the channels. The second one, at higher pressure, reflects the filling of the cavities by nitrogen; this filling occurs at higher pressure the larger the cavity. As can be seen in Figure 3, the second step is shifted to lower pressures as we move from the solvent-extracted sample to the three samples calcined at 700, 800 and 900 °C. This shift in the second step indicates a reduction in the mean size of the cavities as the calcination temperature increases, at least up to 700 °C, in broad agreement with the results obtained from the XRD analysis.

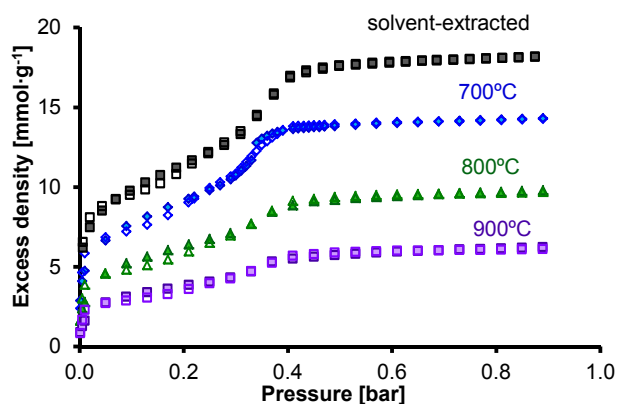


Figure 3: Nitrogen adsorption isotherms at 77 K. Full symbols correspond to experimental results while open symbols represent the predictions from simulation.

There is a progressive decrease in nitrogen adsorption as the calcination temperature increases, although the filling of the cavities takes place at the same pressure. This suggests that the size of the cavities accessible to nitrogen in the samples calcined at 700, 800 and 900 °C is approximately the same, while the number of cavities accessible to nitrogen decreases with the calcination temperature. Thus, the combination of the XRD data and nitrogen adsorption isotherms show that, above a calcination temperature of 700 °C, the main effect of the contraction of the framework is to narrow (or perhaps completely close) at least some of the channels, thereby reducing the accessibility of the cavities to nitrogen.

We now go on to quantify the changing pore structure, already evident from the XRD and nitrogen measurements, using the adsorption-percolation analysis presented in Section 3.

The PSD curves for nitrogen adsorption, obtained by analyzing the adsorption data shown in Figure 3, are shown in Figure 4. All the PSDs have two clear maxima: the first is in the microporous region, reflecting adsorption in the channels, and the second is in the mesoporous region, reflecting adsorption in the cavities. These results confirm the conclusions we drew, above, from inspection of the adsorption isotherms themselves.

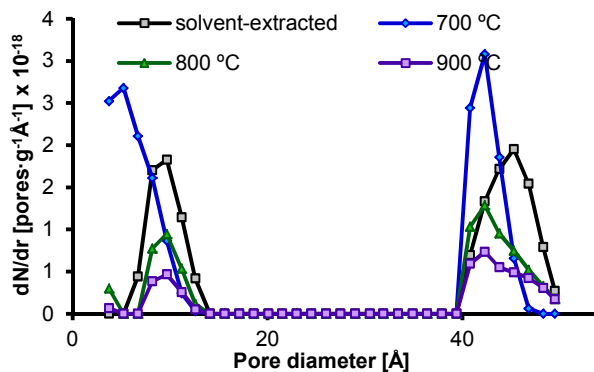


Figure 4: PSDs of SBA-2 samples from nitrogen adsorption at 77 K.

Compared with the solvent-extracted sample, the sample calcined at 700 °C shows a marked reduction in both the size of the cavities and the total pore volume. The pore volume accessible to nitrogen decreases further for the samples calcined at 800 and 900 °C while the mean size of the cavities remains constant. This shows that the reduction in the volume accessible to nitrogen for the materials calcined at the higher temperatures is not caused by a reduction in the size of the cavities, but rather in the degree to which the cavities are accessible to nitrogen.

Table 3 shows the results of the adsorption-percolation analysis for the four samples. There is a clear effect of calcination at higher temperatures on the accessibility of the cavities to nitrogen. The solvent-extracted sample is the most highly connected, with a value of the bond occupation probability ($p^{b,n} = 0.41$), and the corresponding effective coordination number ($z^n = 4.9$, from Equation 1), that are so big that essentially all the cavities are accessible to nitrogen ($P^{s,n} = 1.0$). At 700 °C, the proportion of the cavities that is accessible to nitrogen is only slightly less than unity; $P^{s,n} = 0.975$. Even this relatively small reduction in the accessibility shows that calcination has caused a substantial reduction in the fraction of the channels that are wide enough to accommodate nitrogen molecules, $p^{b,n}$, which is reduced to 0.165 at 700 °C, with a corresponding reduction in z^n . This reflects the form of Figure 1 in which, far from the

percolation threshold, large changes in $p^{b,n}$ (in adsorption terms, the ability of the channels to accommodate the adsorptive species) correspond to small changes in accessibility; this is characteristic of percolation in general. In contrast, as the percolation threshold is closely approached from above, small changes in $p^{b,n}$ lead to the collapse of the accessibility, as we will see below.

Table 3: Unit cell contraction and percolation parameters for nitrogen adsorption at 77 K.

Cal. Temp [°C]	Cell contraction, %	$P^{s,n}$	$p^{b,n}$	z^n
solvent-extracted*	0.0	1.000	0.410	4.90
700	10.7	0.975	0.165	1.98
800	12.1	0.607	0.140	1.68
900	14.1	0.394	0.133	1.59

* From reference 12

As the calcination temperature is increased to 800 and 900 °C, the connectivity of the network progressively decreases, as shown in Table 3. Nevertheless, even for the least well connected network, that of the sample calcined at 900 °C, the network remains above the percolation threshold for the adsorption of nitrogen; at this temperature, $p^{b,n} = 0.133$ and $z^n = 1.59$, whereas the corresponding figures for the percolation threshold are 0.12 and 1.4 respectively.

The experimental adsorption isotherms at 268 K for C4 and isoC4 are shown in Figure 5 and 6, respectively. The isotherms for both hydrocarbons show a step corresponding to the filling of the cavities, as for the nitrogen isotherms.

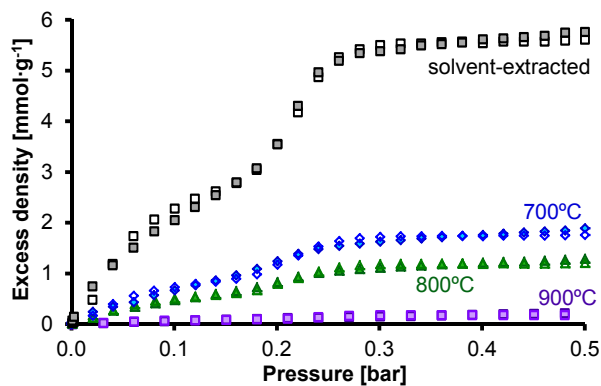


Figure 5: C4 adsorption isotherms at 268 K. Full symbols correspond to experimental results while open symbols represent the predictions from simulation.

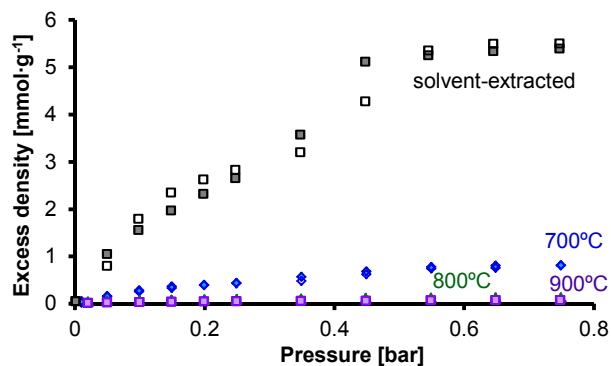


Figure 6: IsoC4 adsorption isotherms at 268 K. Full symbols correspond to experimental results while open symbols represent the predictions from simulation.

The step at low pressure which appeared in the nitrogen isotherms is, however, absent; this reflects the fact that the channels have only a small capacity for the adsorption of larger and more complex C4 and isoC4. It is clear that the dramatic decrease in adsorption capacity for both butane isomers on samples calcined at high temperatures, which is more pronounced than in the case of nitrogen adsorption, cannot be attributed solely to the reduction in unit-cell size. The PSDs are shown in Figures 7 and 8. The adsorption-percolation analysis yields the results shown in Table 4.

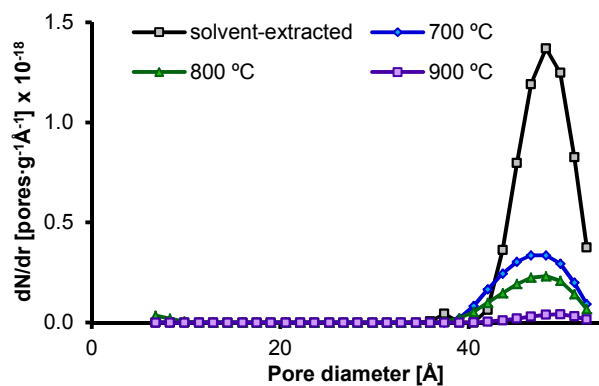


Figure 7: PSDs from C4 adsorption data at 268 K.

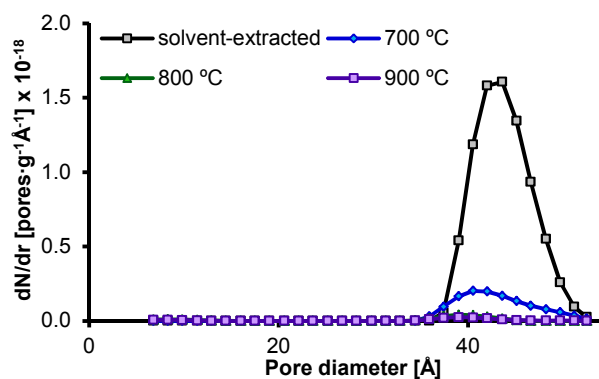


Figure 8: PSDs from isoC4 adsorption data at 268 K.

Table 4: Percolation parameters for butane and isobutane adsorption at 268 K.

Sample	C4			isoC4		
	$P^{s,n}$	$p^{b,C4}$	z^{C4}	$P^{s,n}$	$p^{b,isoC4}$	z^{isoC4}
Solvent-extracted	0.756	0.147	1.76	0.985	0.170	2.04
700	0.250	0.128	1.54	0.155	0.124	1.49
800	0.168	0.125	1.50	0.023	-	-
900	0.023	-	-	0.015	-	-

*The absent values indicate that the pore network of the sample is below its percolation threshold so that – beyond noting that point – no connectivity information can be obtained.

1
2
3
4
5
6
7
8
9
10
11
12
13
14
15
16
17
18
19
20
21
22
23
24
25
26
27
28
29
30
31
32
33
It is clear that the solvent-extracted sample is freely accessible to both C4 and isoC4, as it is to nitrogen; the pore structure does not carry out any sieving of the two butane isomers. Nevertheless, some channels are too small to allow the passage of C4 and isoC4; $p^b = 0.147$ for C4 and 0.170 for isoC4, in comparison to 0.410 for nitrogen¹⁸. [The difference in the values of p^b for C4 and isoC4 indicates that the isoC4 can pass through slightly more channels than can the less bulky isomer, C4. While this is, in principle, an anomalous result, the difference is small compared with the difference between the values of p^b for the two butane isomers, on the one hand, and nitrogen, on the other.] As these values for the bond occupation probability are not yet close to the percolation threshold of the network ($p^b=0.12$), the constrictions in the pore network do not translate to substantially reduced accessibilities and adsorption capacities. In other words, despite the much smaller number of channels that are large enough to allow the passage of the butane isomers, the sub-network formed by these channels is still sufficiently highly connected to allow access to almost all the cavities.

34
35
36
37
38
39
40
41
42
43
44
45
46
47
48
49
50
51
52
53
54
55
56
57
58
59
60
The adsorption-percolation analysis of the samples calcined at higher temperature shows a very different picture. As in the case of the nitrogen results, shown in Table 3, Table 4 shows that there is a substantial reduction in the accessibility of the networks at calcination temperatures of 700 °C and above. This reduction in accessibility, calculated using the adsorption-percolation analysis, reflects the changes in adsorption shown in the isotherms of Figures 5 and 6. At a calcination temperature of 700 °C, while adsorption is less than for the solvent-extracted sample, the adsorption of both isomers remains substantial. The percolation data of Table 4 confirm that the network of the sample calcined at 700 °C is accessible to both isomers. At 800 °C, the adsorption of isoC4 is negligible, while there is still substantial (though much reduced) adsorption of C4. At this temperature, the pore network is accessible to C4 but

1
2
3 inaccessible to isoC4. Expressed in percolation terms, the percolation threshold of the network is
4
5 passed at different calcination temperatures for the two species. At 800 °C, the network is still
6
7 percolating to C4, with 17 % of the cavities accessible and an effective coordination number
8
9 ($z^{b,C4} = 1.5$) just above the percolation threshold ($z^n = 1.4$). For isoC4, in contrast, there is very
10
11 little adsorption and the pore network is below its percolation threshold. At the still higher
12
13 calcination temperature of 900 °C, Table 4 shows that the pore network of the sample is below
14
15 the percolation threshold for both butane isomers; the adsorption of both isomers is negligible.
16
17 In contrast, as we showed above, the pore network remains accessible to nitrogen even at this
18
19 highest calcination temperature.
20
21
22
23

24 This behavior suggests the possibility of using the calcination process to fine-tune the
25
26 accessibility to the SBA-2 mesoporous structure of different adsorptives, in order to achieve a
27
28 molecular-sieving effect. For the system we have studied in the present paper, we know that
29
30 calcination temperatures above about 700 °C give SBA-2 samples that have a substantial
31
32 capacity for the adsorption of pure C4, and a very low capacity for the adsorption of isoC4,
33
34 because the latter molecule does not significantly penetrate the pore network. This suggests that,
35
36 in adsorption from a mixture of these two species, this material should selectively adsorb C4
37
38 over isoC4 – in other words it would exhibit molecular sieving of the branched alkane allowing
39
40 the linear alkane to adsorb. The separation of normal and iso-alkanes is an important industrial
41
42 adsorption process²⁸, and the combination of the high capacity of SBA-2 materials – due to the
43
44 cavities – and the tunable molecular sieving – due to the channels – is of potential industrial
45
46 interest. More fundamentally, this would be an illustration of the separation manipulation of
47
48 pore-size and connectivity effects in the design of porous materials. To test our hypothesis, we
49
50 have carried out mixture adsorption experiments with a mixture of C4 and isoC4, using two
51
52
53
54
55
56
57
58
59
60

1
2
3 samples of SBA-2 – one calcined at 550 °C and one at 820 °C. The effectiveness of this
4
5 separation can be quantified in terms of the selectivity of the material for C4 over isoC4, defined
6
7 as
8

$$S = \frac{x/(1-x)}{y/(1-y)} \quad (3)$$

9
10
11
12
13 where x and y are the mole fractions of C4 (the more strongly adsorbed species) in the adsorbed
14
15 phase and in the bulk-gas phase respectively. Based on our observation that the capacity of SBA-
16
17 2 for isoC4 becomes very small at calcination temperatures above about 700 °C, we would
18
19 expect the selectivity to be very high for the sample calcined at 820 °C. This is confirmed by the
20
21 mixture adsorption measurements, in which we found $S = 510$ for calcination at 820 °C, and $S =$
22
23 6.6 for calcination at 550 °C. The latter value reflects the adsorption selectivity of the essentially
24
25 unconstricted SBA-2 network for C4 over isoC4. It follows, therefore, that the constriction of
26
27 the pore network caused by calcination at high temperature, leading to the network becoming
28
29 largely inaccessible to isoC4, increases the selectivity by a factor of about 100.
30
31
32
33
34
35
36

37 5. CONCLUSIONS

38
39 Our study of the adsorption of nitrogen and the two butane isomers on a series of SBA-2
40
41 materials calcined at different temperatures gives a clear picture of changes in the pore structure
42
43 as the calcination temperature increases. The adsorption-percolation analysis shows that the
44
45 network becomes increasingly constricted as the calcination temperature increases, reducing the
46
47 accessibility of the network to all three species studied. The more bulky the molecule, the more
48
49 susceptible it is to these constrictions. While the SBA-2 pore network remains accessible to
50
51 nitrogen even at the highest calcination temperature, 900 °C, it becomes inaccessible to isoC4 at
52
53
54
55
56
57
58
59
60

1
2
3 a lower calcination temperature than is the case for C4. The long-range order of SBA-2 remains
4
5 intact even at the highest calcination temperature.
6
7

8 The fact that the two butane isomers have a different percolation threshold, as a function of the
9
10 calcination temperature, suggests using the calcination temperature as a design parameter, the
11
12 tuning of which could give an adsorbent with a high selectivity for the C4/isoC4 separation (and,
13
14 in principle, for other separations of linear and branched hydrocarbons). Our mixture adsorption
15
16 measurements confirmed that this effect occurs in practice. SBA-2 thus demonstrates an
17
18 interesting combination of high adsorption capacity, due to the cavities, and a molecular sieving
19
20 effect, due to the channels connecting the cavities. Furthermore, it should be possible to
21
22 generalize this approach to tune the window size of mesoporous solids containing cages to
23
24 optimize molecular selectivity for molecules of sizes extending into the nanometer regime,
25
26 where the pores of zeolites – conventionally used for molecular-sieving applications – would be
27
28 too small to allow uptake.
29
30
31
32
33

34 35 36 ASSOCIATED CONTENT

37
38
39 Nitrogen adsorption isotherms of SBA-2 solvent-extracted and calcined at 550 °C¹⁶ and TEM
40
41 micrographs of SBA-2 solid calcined at 900 °C are available as supporting information. This
42
43 material is available free of charge via the Internet at <http://pubs.acs.org>.
44
45
46

47 48 AUTHOR INFORMATION

49 50 Corresponding Author

51
52
53 Manuel Pérez-Mendoza. University of Granada. E-mail contact: mjperezm@ugr.es
54
55

56 57 Present Addresses

58
59
60

1
2
3
4
5
6
7
8
9
10
11
12
13
14
15
16
17
18
19
20
21
22
23
24
25
26
27
28
29
30
31
32
33
34
35
36
37
38
39
40
41
42
43
44
45
46
47
48
49
50
51
52
53
54
55
56
57
58
59
60

✧ Prof. Nigel A. Seaton: Abertay University, Dundee DD1 1HG, United Kingdom.

* Dr. David Fairen-Jiménez: Department of Chemical Engineering & Biotechnology, University of Cambridge, Pembroke Street, Cambridge, CB2 3RA, UK.

ACKNOWLEDGMENT

We thank the DeSSANS project (EU FP6 STREP SES6CT2005-020133) and The University of Edinburgh for financial support. J. González also acknowledges financial support from **FRABA-** Universidad de Colima 761/11

REFERENCES

(1) Kresge, C. T.; Leonowicz, M. E.; Roth, W. J.; Vartuli, J. C.; Beck, J. S. Ordered Mesoporous Molecular-Sieves Synthesized by a Liquid-Crystal Template Mechanism. *Nature* **1992**, *359* (6397), 710-712.

(2) Beck, J. S.; Vartuli, J. C.; Roth, W. J.; Leonowicz, M. E.; Kresge, C. T.; Schmitt, K. D.; Chu, C. T. W.; Olson, D. H.; Sheppard, E. W.; McCullen, S. B., et al. A New Family of Mesoporous Molecular-Sieves Prepared with Liquid-Crystal Templates. *J. Am. Chem. Soc.* **1992**, *114* (27), 10834-10843.

(3) Ciesla, U.; Schuth, F. Ordered Mesoporous Materials. *Microporous Mesoporous Mater.* **1999**, *27* (2-3), 131-149.

(4) Yiu, H. H. P.; Wright, P. A. Enzymes Supported on Ordered Mesoporous Solids: A Special Case of an Inorganic-Organic Hybrid. *J. Mater. Chem.* **2005**, *15* (35-36), 3690-3700.

(5) Garcia-Bennett, A. E. Synthesis, Toxicology and Potential of Ordered Mesoporous Materials in Nanomedicine. *Nanomedicine* **2011**, *6* (5), 867-877.

1
2
3 (6) Beck, J. S.; Vartuli, J. C.; Kennedy, G. J.; Kresge, C. T.; Roth, W. J.; Schramm, S. E.
4
5 Molecular or Supramolecular Templating - Defining the Role of Surfactant Chemistry in the
6
7 Formation of Microporous and Mesoporous Molecular-Sieves. *Chem. Mater.* **1994**, *6* (10), 1816-
8
9 1821.

10
11
12
13 (7) Zhao, D. Y.; Huo, Q. S.; Feng, J. L.; Chmelka, B. F.; Stucky, G. D. Nonionic Triblock and
14
15 Star Diblock Copolymer and Oligomeric Surfactant Syntheses of Highly Ordered,
16
17 Hydrothermally Stable, Mesoporous Silica Structures. *J. Am. Chem. Soc.* **1998**, *120* (24), 6024-
18
19 6036.

20
21
22
23 (8) Van der Voort, P.; Mathieu, M.; Mees, F.; Vansant, E. F. Synthesis of High-Quality Mcm-
24
25 48 and Mcm-41 by Means of the Gemini Surfactant Method. *J. Phys. Chem. B* **1998**, *102* (44),
26
27 8847-8851.

28
29
30
31 (9) Tanev, P. T.; Pinnavaia, T. J. A Neutral Templating Route to Mesoporous Molecular-
32
33 Sieves. *Science* **1995**, *267* (5199), 865-867.

34
35
36
37 (10) Park, S. S.; Ha, C. S. Organic-Inorganic Hybrid Mesoporous Silicas: Functionalization,
38
39 Pore Size, and Morphology Control. *Chemical Record* **2006**, *6* (1), 32-42.

40
41
42
43 (11) Angloher, S.; Bein, T., *Organic Functionalisation of Mesoporous Silica*. ELSEVIER
44
45 SCIENCE BV: AMSTERDAM, 2005; p 2017-2026.

46
47
48
49 (12) Hunter, H. M. A.; Garcia-Bennett, A. E.; Shannon, I. J.; Zhou, W. Z.; Wright, P. A.
50
51 Particle Morphology and Microstructure in the Mesoporous Silicate Sba-2. *J. Mater. Chem.*
52
53 **2002**, *12* (1), 20-23.
54
55
56
57
58
59
60

1
2
3 (13) Zhou, W. Z.; Hunter, H. M. A.; Wright, P. A.; Ge, Q. F.; Thomas, J. M. Imaging the Pore
4 Structure and Polytropic Intergrowths in Mesoporous Silica. *J. Phys. Chem. B* **1998**, *102* (36),
5 6933-6936.
6
7

8
9
10 (14) Perez-Mendoza, M.; Gonzalez, J.; Wright, P. A.; Seaton, N. A. Elucidation of the Pore
11 Structure of Sba-2 Using Monte Carlo Simulation to Interpret Experimental Data for the
12 Adsorption of Light Hydrocarbons. *Langmuir* **2004**, *20* (18), 7653-7658.
13
14
15

16 (15) Han, L.; Sakamoto, Y.; Terasaki, O.; Li, Y.; Che, S. Synthesis of Carboxylic Group
17 Functionalized Mesoporous Silicas (Cfmss) with Various Structures. *J. Mater. Chem.* **2007**, *17*
18 (12), 1216-1221.
19
20
21

22 (16) Ma, Y. H.; Han, L.; Miyasaka, K.; Oleynikov, P.; Che, S. N.; Terasaki, O. Structural
23 Study of Hexagonal Close-Packed Silica Mesoporous Crystal. *Chem. Mater.* **2013**, *25* (10),
24 2184-2191.
25
26
27

28 (17) Ferreiro-Rangel, C. A.; Lozinska, M. M.; Wright, P. A.; Seaton, N. A.; Duren, T. Kinetic
29 Monte Carlo Simulation of the Synthesis of Periodic Mesoporous Silicas Sba-2 and Stac-1:
30 Generation of Realistic Atomistic Models. *J. Phys. Chem. C* **2012**, *116* (39), 20966-20974.
31
32
33

34 (18) Perez-Mendoza, M.; Gonzalez, J.; Wright, P. A.; Seaton, N. A. Structure of the
35 Mesoporous Silica SBA-2, Determined by a Percolation Analysis of Adsorption. *Langmuir* **2004**,
36 *20* (22), 9856-9860.
37
38
39

40 (19) Yanuka, M. Percolation Theory and Capilarity in Relation to Pore Geometry. University
41 of Guelph, 1984.
42
43
44
45
46
47
48
49
50
51
52
53
54
55
56
57
58
59
60

1
2
3 (20) Yun, J. H.; Duren, T.; Keil, F. J.; Seaton, N. A. Adsorption of Methane, Ethane, and Their
4 Binary Mixtures on Mcm-41: Experimental Evaluation of Methods for the Prediction of
5 Adsorption Equilibrium. *Langmuir* **2002**, *18* (7), 2693-2701.
6
7

8
9
10
11 (21) Kjems, J. K.; Dolling, G. Crystal Dynamics of Nitrogen - Cubic Alpha-Phase. *Phys. Rev.*
12 *B* **1975**, *11* (4), 1639-1647.
13
14

15
16
17 (22) Bezus, A. G.; Kiselev, A. V.; Lopatkin, A. A.; Du, P. Q. Molecular Statistical Calculation
18 of Thermodynamic Adsorption Characteristics of Zeolites Using Atom-Atom Approximation .1.
19 Adsorption of Methane by Zeolite Nax. *J. Chem. Soc. Faraday Trans.* **1978**, *74*, 367-379.
20
21
22

23
24 (23) Jorgensen, W. L.; Madura, J. D.; Swenson, C. J. Optimized Intermolecular Potential
25 Functions for Liquid Hydrocarbons. *J. Am. Chem. Soc.* **1984**, *106* (22), 6638-6646.
26
27
28

29
30 (24) Lorenz, C. D.; May, R.; Ziff, R. M. Similarity of Percolation Thresholds on the Hcp and
31 Fcc Lattices. *J. Stat. Phys.* **2000**, *98* (3-4), 961-970.
32
33
34

35
36 (25) Davies, G. M.; Seaton, N. A.; Vassiliadis, V. S. Calculation of Pore Size Distributions of
37 Activated Carbons from Adsorption Isotherms. *Langmuir* **1999**, *15* (23), 8235-8245.
38
39
40

41 (26) Gonzalez, J. PhD Thesis University of St. Andrews, 2005.
42
43

44 (27) Huo, Q. S.; Leon, R.; Petroff, P. M.; Stucky, G. D. Mesostucture Design with Gemini
45 Surfactants - Supercage Formation in a 3-Dimensional Hexagonal Array. *Science* **1995**, *268*
46 (5215), 1324-1327.
47
48
49

50 (28) Yang, R. T., *Gas Separation by Adsorption Processes*. Imperial College Press: 1987.
51
52
53
54
55
56
57
58
59
60

TABLE OF CONTENTS

